.

Microscopic four-point-probe resistivity measurements of shallow, high density doping layers in silicon

Craig M. Polley' , Warrick R. Clarke, Jill A. Miwa, Michelle Y. Simmons, and Justin W. Wells

Citation: Appl. Phys. Lett. **101**, 262105 (2012); doi: 10.1063/1.4773485
View online: http://dx.doi.org/10.1063/1.4773485
View Table of Contents: http://aip.scitation.org/toc/apl/101/26
Published by the American Institute of Physics

RIGHTSLINK

APPLIED PHYSICS LETTERS **101**, 262105 (2012)

Microscopic four-point-probe resistivity measurements of shallow, high density doping layers in silicon

Craig M. Polley,[1,a)] Warrick R. Clarke,[1] Jill A. Miwa,[1] Michelle Y. Simmons,[1] and Justin W. Wells[2]
[1]*School of Physics, University of New South Wales, Sydney, Australia*
[2]*Department of Physics, NTNU, Trondheim, Norway and MAX IV Laboratory, Lund University, Lund, Sweden*

(Received 2 November 2012; accepted 13 December 2012; published online 28 December 2012)

We present room temperature resistivity measurements of shallow, monolayer doped phosphorus in silicon, a material system of interest for both conventional microelectronic manufacturing, and future quantum electronic devices. Using an *in-situ* variable spacing microscopic four-probe system, we demonstrate the ability to separate the conductivity of the substrate and the doping layer. We show that the obtained sensitivity to the dopant layer derives from a combination of the nanoscale contacting areas and the conductivity difference between the highly doped 2D layer and the substrate. At an encapsulation depth of only 4 nm, we demonstrate a room temperature resistivity of 1.4 kΩ/□.
© *2012 American Institute of Physics*. [http://dx.doi.org/10.1063/1.4773485]

In recent years, the development of ultra-high vacuum (UHV) four-point probes (4PP) has enabled conductance measurements of a wide range of surface material systems.[1–4] As microelectronic manufacturing scales to a sub-10 nm scale,[5] the ultra-shallow silicon doping required for transistor source/drain extensions is fast becoming a system where surface interactions are important. There is hence interest in applying microscopic 4PP systems to their sheet resistance characterization.[6] Here, we present a study of the resistivity of 4 nm deep phosphorus δ-doping layers in silicon at room temperature. In addition to yielding highly dense, abrupt doping profiles attractive for ultra-shallow junction applications, this material system is also an important component of proposed quantum computer architectures.[7,8]

However, these applications demand the use of substrates which are conductive at room temperature, and it is not obvious that 4PP resistivity measurements are possible without significant error due to leakage current through the substrate. In this material system, it is not possible to employ common methods for eliminating substrate conduction such as using insulating substrates,[2] resistive surface space-charge layers,[9] or rectifying tip-sample contacts.[1,10] Nonetheless, we are able to demonstrate 4PP resistivity measurements on conductive substrates (nominal doping 1–10 Ωcm) which are clearly unaffected by conduction through the substrate. We show that this can be explained from consideration of the different spreading resistances to each layer and is chiefly determined by the nanoscale contact area of each probe combined with the bulk:2D-layer conductivity ratio. These results highlight that one cannot always ignore two-terminal resistances when performing four-terminal resistance measurements.

For these experiments, we have used both n- and p-type Si(100) substrates, with doping densities spanning 0.02 to 130 Ωcm. Clean, 2×1 reconstructed silicon surfaces were prepared by heating samples to 1200 °C in UHV. The reconstructed surfaces were then saturation dosed with 1.4 L of phosphine gas at room temperature and annealed to 350 °C for 60 s to substitutionally incorporate phosphorus atoms into the top layer of the silicon lattice.[11] The incorporated surfaces were then held at 250 °C and overgrown with epitaxial silicon from a high-resistivity (>1 kΩcm) sublimation cell at a growth rate of ≈ 3 Å/min. These growth parameters have been shown previously to optimize the transport properties[12] and minimize the segregation length (0.6 nm (Ref. 13)) of the doping profile. At such low temperatures and in the absence of crystal damage, dopant diffusion is essentially negligible. With 25 nm of encapsulation, this process is known to result in full dopant activation, with very high 2D carrier densities of $\approx 2 \times 10^{14}$ cm^{-2}.[14]

Here, we capitalize on the *in-situ* measurement system and focus on near-surface layers with ≈ 4 nm of encapsulation. An Omicron Nanoprobe UHV 4PP system was used to perform resistivity measurements before and after δ-doping the substrates. Four tungsten probes were configured in a collinear arrangement as shown in Fig. 1, with equidistant probe spacings s of 50–200 μm. A lateral probe positioning accuracy of $\pm 2\%$ is realized using a scanning electron microscope (SEM). The probes have contact radii of <100 nm (as directly verified by *in-* and *ex-situ* SEM imaging) and are approached to the surface as 4 independent scanning tunnelling microscope tips with electrical feedback control to avoid damaging either the sample or the probes. Once a feedback-controlled tunnelling contact is established, we disengage the feedback and further approach the probes with manual fine-motion piezo control until a sufficient measurement current is obtained. This results in a physical contact, but with the *in-situ* SEM imaging, we can confirm that there is no observable damage to the sample nor any inelastic deformation of the probes. We then sweep a direct current between the outer probes and record the potential across both the inner and outer probe pairs, obtaining voltage-current traces as shown in Fig. 1. The gradients of these different traces give the four-terminal (R_{4T}) and two-terminal (R_{2T}) resistance, respectively.

The four-terminal resistance R_{4T} can be used to determine the sample resistivity ρ by using Laplace's equation[15]

[a)]craig.polley@gmail.com.

 © 2012 American Institute of Physics

RIGHTSLINK

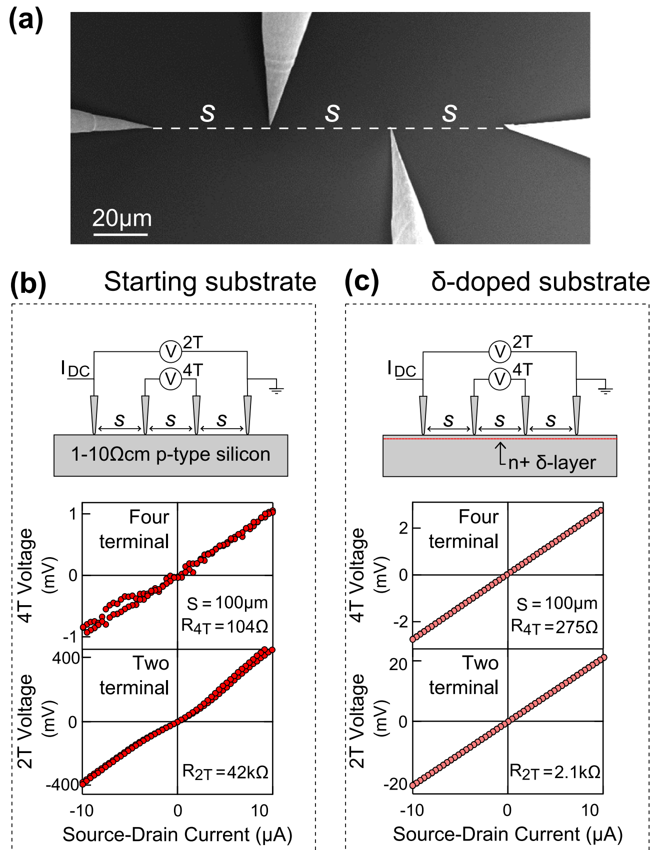

FIG. 1. (a) Collinear four probe resistance measurements of bulk doped silicon substrates and highly doped, shallow Si:P dopant layers. V–I characteristics are shown for a 1–10 Ωcm p-type substrate before (b) and after (c) phosphine dosing and encapsulation with 4 nm of epitaxial silicon.

$$R_{4T} = \frac{\rho}{2\pi s F_1} \quad (3D), \tag{1}$$

where s is the probe spacing and F_1 a correction factor for the finite sample thickness t[15]

$$F_1 = \frac{t/s}{2\ln\left(\frac{\sinh(t/s)}{\sinh(t/2s)}\right)}. \tag{2}$$

At the limit of an infinitely deep substrate ($t \gg s$) F_1 tends to 1, while for strictly 2D conduction ($t \ll s$), Eq. (1) is reduced to

$$R_{4T} = \frac{\rho_s \ln(2)}{\pi} \quad (2D). \tag{3}$$

Equations (1) and (3) differ in their functional dependence on the probe spacing, such that a measurement performed as a function of s easily distinguishes transport through the bulk ($R \propto 1/s$) and the dopant layer ($R = $ constant).[9,16,17]

With a similar application of the Laplace equation, the two-terminal resistance can be related to the probe spacing, sample resistivity, and probe contact radii r

$$R_{2T} = \begin{cases} \frac{\rho}{\pi}\left(\frac{1}{r} - \frac{1}{3s-r}\right) & (3D) \\ \frac{\rho_s}{\pi}\ln\left(\frac{3s-r}{r}\right) & (2D) \end{cases}. \tag{4}$$

This model encompasses what is often referred to as spreading resistance, in which constricted current flow close to the source and drain contacts is considered. Since typically $r \ll s$, for both the 3D and 2D cases the two-terminal resistance is dominated by the sample resistivity and the probe radii. In reality, this model provides only a lower bound, since it does not include interfacial contact resistance and assumes indenting contacts.

Before forming a Si:P δ-layer, the 1–10 Ωcm p-type Si(100) sample in Fig. 1 had a four-terminal resistance of 104 Ω at a probe spacing of 100 μm (Fig. 1(b)), as expected from Eq. (1) and the nominal substrate resistivity. The two-terminal resistance ($R_{2T} \approx 42$ kΩ) is two orders of magnitude higher due to the inclusion of interfacial and spreading resistance. After phosphine dosing and encapsulating with 4 nm of silicon, the two-terminal resistance reduces by a factor of 20 (Fig. 1(c)), suggesting an additional transport path or a large improvement in contact resistance due to the introduction of a highly doped layer at the surface. The *increase* in four-terminal resistance from 104 Ω to 275 Ω is potentially counter intuitive but implies that conduction is now dominated by transport through the 2D δ-layer.

To investigate this further, we repeated the resistance measurements as a function of probe spacing across three different Si(100) substrates: 300 μm thick 1–10 Ωcm p-type, 300 μm thick 1–10 Ωcm n-type, and 2 μm thick 5 Ωcm p-type silicon-on-insulator (SOI). Since probe spacing dependent resistance measurements indicate whether transport is 2D or 3D, we can identify the influence of the substrate on the measured conduction. These three substrate types were chosen in order to vary both the substrate doping type (p vs. n) and dimensionality (bulk vs. SOI). In Fig. 2, we show the four-terminal resistances R_{4T} as a function of probe spacing for these three substrate types, before and after phosphine dosing and

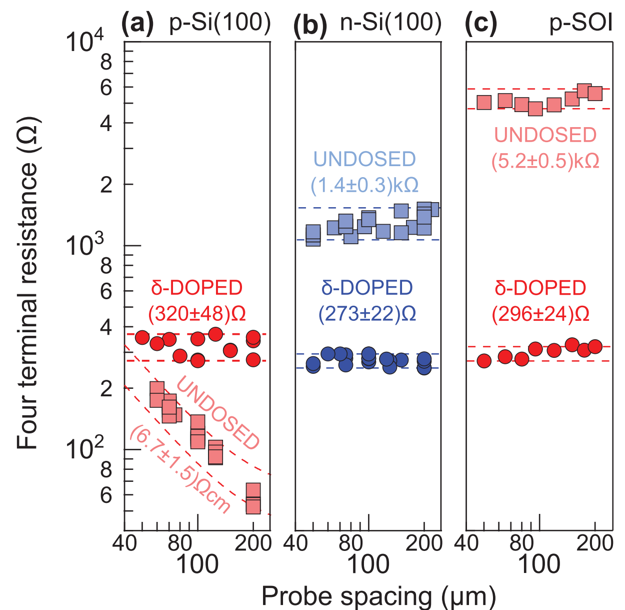

FIG. 2. Probe spacing dependence of the four-terminal resistance of three different silicon substrates, before and after phosphorus δ-doping. The substrates are (a) 300 μm thick 1–10 Ωcm p-type, (b) 300 μm thick 1–10 Ωcm n-type, and (c) 2 μm thick 5 Ωcm p-type silicon-on-insulator. For all samples, the encapsulation thickness after δ-doping is (4.0 ± 0.5) nm.

RIGHTSLINK

encapsulating. In each case, the data have been taken from several different samples to ensure reproducibility.

We first establish that before δ-doping, all substrates behave as expected for their respective dimensions and doping levels. The bulk p-type samples in Fig. 2(a) show a resistance inversely proportional to the probe spacing. Fitting this with Eq. (1) yields a bulk resistivity of $(6.7\pm1.5)\,\Omega$cm, in agreement with the nominal doping level of 1–10 Ωcm.

The bulk n-type samples in Fig. 2(b) show much higher resistance than the bulk p-type samples, despite having a comparable bulk doping density. As has been previously reported, this is due to the presence of a high resistivity inversion layer, which in turn is a consequence of Fermi level pinning at the surface.[9,18] In the case of 2×1 reconstructed Si(100), photoemission measurements have demonstrated that the surface Fermi level is pinned at ≈ 0.34 eV above the valence band edge by surface states,[19,20] A consequence of this effect is that n-type substrates possess a surface inversion layer, electrically isolating the conductive bulk substrate and limiting conduction to a resistive surface layer a few hundred nanometers thick. This is the origin of the large ($\approx$kΩ), probe spacing independent resistance observed in Fig. 2(b). This effect is unique to microscopic UHV 4PP systems, since more conventional 4PP systems employ a much higher contacting load (>10 g) which causes both deeper penetration of the probes into the substrate and the creation of metallic β-Sn phase silicon,[21] forming local Ohmic contacts.

Finally, the SOI sample of Fig. 2(c) has a 2 μm thick device layer, which remains effectively 2D for the range of probe spacings used here. From this, we obtain a four-terminal resistance of (5.2 ± 0.5) kΩcm, again independent of probe spacing and in agreement with that predicted from the nominal resistivity and thickness of the silicon layer.

Having established the transport behaviour of the substrates before δ-doping, we now examine changes introduced by saturation dosing the samples with phosphine, substitutionally incorporating the P dopants into the crystal lattice and then encapsulating with 4 nm of epitaxial silicon. Following such a process, we create a sharp, high density quantum well in the plane of the dopants, and the resistance measurements change significantly. Where previously four-terminal resistances spanned 2 orders of magnitude across the three different substrate types, they now all converge to (310 ± 60) Ω for all probe spacings. The resistance is now independent of both the probe spacing and the properties of the underlying substrate, demonstrating that substrate conduction no longer plays a dominant role in transport. We note that for any single sample, the resistance variation is typically better than $\pm20\,\Omega$. In Fig. 2, we have combined the results of many separate sample preparations, giving rise to a larger measurement variance.

It is not intuitively obvious why the measurements are unaffected by substrate leakage. Previous studies have highlighted the difficulties in measuring ultra-shallow doping structures where parallel transport through the substrate is a critical issue.[22] In particular, while the absence of leakage through p-type substrates can be rationalized by the formation of a p-n inversion layer, this cannot explain the measurements on n-type substrates where we have an n^+/n doping structure. This is an archetypal Ohmic contact, and we would expect excellent electrical contact to the substrate.

To understand this result, we must consider the *two-terminal* (i.e., source-to-drain) resistances of the δ-doping layer and of the substrate, as given by Eq. (4). For such a system, it is the ratio of two-terminal resistances between the highly doped layer and the substrate which determines the preferred current path; four-terminal resistances alone cannot be used to determine which layer should dominate conduction. This is an important conceptual point—typically in a four terminal measurement only the total amount of current matters, not how this current enters and exits the sample. But in cases where there are multiple possible current paths in the sample, the distribution of current can depend on how it is sourced and drained.

Therefore, whilst it might be expected that a δ-doping layer would serve as an excellent contact to the underlying substrate, these microscopic 4PP measurements are strongly influenced by the spreading resistance of the source and drain probes. In this case, the result is that the δ-doping layer is the preferred current path. To illustrate this, in Fig. 3(a)

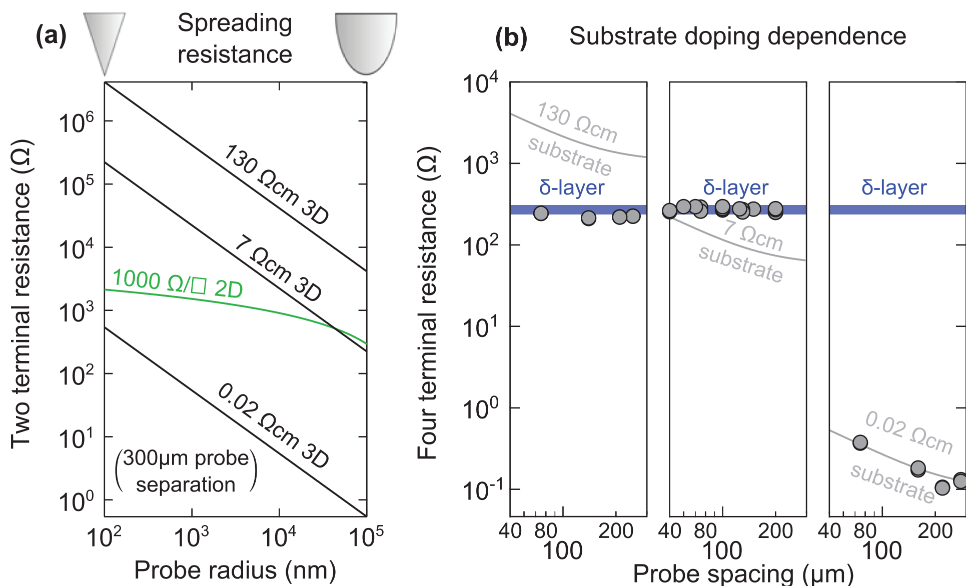

FIG. 3. The significance of two-terminal resistance in bulk sensitivity. (a) The predicted two-terminal source-to-drain resistances as a function of probe radius for a variety of substrate doping levels at a fixed probe spacing of 300 μm (from Eq. (4)). For the $\approx$ 100 nm radius probes used here, the 2D δ-layer (green trace) is $\approx100\times$ more conductive than the 7 Ωcm bulk substrate. (b) Experimental four-terminal resistances (grey circles) of δ-layers on different n-type substrates with varying doping densities confirm the predictions of (a). 2D conduction is still observed on a much lower doped (130 Ωcm) substrate, but bulk conduction dominates on a much heavier doped (20 mΩcm) substrate.

RIGHTSLINK

we plot theoretical two-terminal resistances (Eq. (4)) as a function of the probe radius for a $1\,\mathrm{k}\Omega/\square$ 2D layer (green trace), the same resistivity of the δ-layer in Fig. 2. We also plot similar traces for 3D substrates of different doping densities (130, 7, and $0.02\,\Omega$cm). The two-terminal resistance increases as the measurement probes become sharper (the so-called spreading resistance), but this increase is much steeper for the 3D substrates compared to the 2D δ-layer. As a consequence, for the ≈ 100 nm radius probes typically used in our experiments, the δ-layer is ≈ 100 times more conductive than the $7\,\Omega$cm bulk substrate it is created on, and hence the δ-layer dominates conduction.

To verify that this interpretation is correct, we have performed similar δ-doping measurements using much higher ($130\,\Omega$cm) and lower ($20\,\mathrm{m}\Omega$cm) resistivity n-type substrates. Considering the spreading resistance model in Fig. 3(a), we expect no change in the four-terminal resistance on a more resistive ($130\,\Omega$cm) substrate, since the δ-layer is now ≈ 1000 times more conductive than the substrate. However on the less resistive $20\,\mathrm{m}\Omega$cm substrate, the resistance ratio is reversed, with the bulk now 10–100 times more conductive than the δ-layer. In this limit, we thus expect four-probe measurements to revert to the bulk 3D relationship with probe spacing (Eq. (1)). Experimental data shown in Fig. 3(b) matches these expectations. The light grey curves illustrate the expected four-terminal resistances of the substrate alone, while the blue curves indicate the expected resistance of a 4 nm deep δ-layer as given by Fig. 2. As can be seen, measurements of 4 nm deep layers (grey circles) are unchanged when the substrate resistivity is increased from 7 to $130\,\Omega$cm, while for the $20\,\mathrm{m}\Omega$cm substrate bulk conduction dominates. This confirms that our measurement results in Fig. 2 on $1–10\,\Omega$cm substrates are dominated by transport through the δ-doping layer alone and can be readily converted into a sheet resistivity using Eq. (3). Doing so, we obtain a sheet resistance of $1.4\,\mathrm{k}\Omega/\square$, which at a nominal depth of only 4 nm from the surface exceeds both future targets for microelectronic manufacturing[5] and previously reported monolayer doping studies.[23]

In conclusion, we have shown that robust, reliable 4PP conductance measurements of shallow doping layers are possible even when using conducting substrates. This is by virtue of a spreading resistance effect and can be shown to depend on both the probe radii and the bulk:2D-layer conductivity ratio. Measuring high-density phosphorus δ-layers in silicon, we obtain a resistivity of $1.4\,\mathrm{k}\Omega/\square$ at a nominal depth of only 4 nm from the surface. Moreover, the approach presented here permits study of the conductivity of monolayer doping profiles at arbitrarily shallow depths, of particular interest for investigations into the limits of ultra-shallow junction scaling.

C.M.P. thanks Giordano Scappucci and Giovanni Capellini for insightful discussions. This research was conducted by the Australian Research Council Centre of Excellence for Quantum Computation and Communication Technology (project number CE110001029). W.R.C. acknowledges funding from the Australian Research Council in the form of an Australian Post-Doctoral Fellowship. M.Y.S. acknowledges an Australian Government Federation Fellowship.

[1]A. S. Walton, C. S. Allen, K. Critchley, M. L. Górzny, J. E. McKendry, R. M. D. Brydson, B. J. Hickey, and S. D. Evans, Nanotechnology **18**, 065204 (2007).
[2]S.-H. Ji, J. B. Hannon, R. M. Tromp, V. Perebeinos, J. Tersoff, and F. M. Ross, Nature Mater. **11**, 114 (2012).
[3]F. Song, L. Gammelgaard, Ph. Hofmann, and J. W. Wells, Appl. Phys. Lett. **98**, 052106 (2011).
[4]T. Hirahara, Y. Sakamoto, Y. Saisyu, H. Miyazaki, S. Kimura, T. Okuda, I. Matsuda, S. Murakami, and S. Hasegawa, Phys. Rev. B **81**, 165422 (2010).
[5]2011 International Technology Roadmap for Semiconductors, Table FEP12.
[6]D. H. Petersen, O. Hansen¸ T. M. Hansen, P. Bøggild, R. Lin, D. Kjær, P. F. Nielsen, T. Clarysse, W. Vandervorst, E. Rosseel, N. S. Bennett, and N. E. B. Cowern, J. Vac. Sci. Technol. B **28**, C1C27 (2010).
[7]M. Fueschle, J. A. Miwa, S. Mahapatra, H. Ryu, S. Lee, O. Warschkow, L. C. L. Hollenberg, G. Klimeck, and M. Y. Simmons, Nat. Nanotechnol. **7**, 242 (2012).
[8]S. Mahapatra, H. Büch, and M. Y. Simmons, Nano Lett. **11**, 4376 (2011).
[9]C. Liu, I. Matsuda, S. Yoshimoto, T. Kanagawa, and S. Hasegawa, Phys. Rev. B **78**, 035326 (2008).
[10]V. Cherepanov, E. Zubkov, H. Junker, S. Korte, M. Blab, P. Coenen, and B. Voigtländer, Rev. Sci. Instrum. **83**, 033707 (2012).
[11]S. R. Schofield, N. J. Curson, M. Y. Simmons, F. J. Reuß, T. Hallam, L. Oberbeck, and R. G. Clark, Phys. Rev. Lett. **91**, 136104 (2003).
[12]K. E. J. Goh, L. Oberbeck, M. Y. Simmons, A. R. Hamilton, and R. G. Clark, Appl. Phys. Lett. **85**, 4953 (2004).
[13]L. Oberbeck, N. J. Curson, T. Hallam, M. Y. Simmons, G. Bilger, and R. G. Clark, Appl. Phys. Lett. **85**, 1359 (2004).
[14]S. R. McKibbin, W. R. Clarke, A. Fuhrer, T. C. G. Reusch, and M. Y. Simmons, Appl. Phys. Lett. **95**, 233111 (2009).
[15]D. K. Schroder, *Semiconductor Material and Device Characterization* (John Wiley & Sons, 1990), p. 2.
[16]J. W. Wells, J. F. Kallehauge, T. M. Hansen, and Ph. Hofmann, Phys. Rev. Lett. **97**, 206803 (2006).
[17]J. W. Wells, K. Handrup, J. F. Kallehauge, L. Gammelgaard, P. Bøggild, M. B. Balslev, J. E. Hansen, P. R. E. Petersen, and Ph. Hofmann, J. Appl. Phys. **104**, 053717 (2008).
[18]Ph. Hofmann and J. W. Wells, J. Phys. Condens. Matter. **21**, 013003 (2009).
[19]F. J. Himpsel, P. Heimann, T. C. Chiang, and D. E. Eastman, Phys. Rev. Lett. **45**, 1112 (1980).
[20]P. Mårtensson, A. Cricenti, and G. V. Hansson, Phys. Rev. B **33**, 8855 (1986).
[21]T. Clarysse, P. DeWolf, H. Bender, and W. Vandervorst, J. Vac. Sci. B **14**, 358 (1996).
[22]T. Clarysse, D. Vanhaeren, and W. Vandervorst, J. Vac. Sci. Technol. B **20**, 459 (2002).
[23]J. C. Ho, R. Yerushalmi, G. Smith, P. Majhi, J. Bennet, J. Halim, V. N. Faifer, and A. Javey, Nano Lett. **9**, 725 (2009).

RIGHTSLINK Copyright Clearance Center